Design of Sliding-Mode Speed Controller With Active Damping Control for Single-Inverter Dual-PMSM Drive Systems

Tae-Il Yeam, *Student Member, IEEE*, and Dong-Choon Lee, *Senior Member, IEEE*

***Abstract*—In this article, a novel sliding mode speed controller is proposed for the parallel operation of dual permanent magnet synchronous motors (PMSMs) with a single inverter. For this operation, the vector control method is applied to the master motor drive and the open-loop control mode is employed for the slave one. If the load torques of two motors are different, oscillations in the speed of the slave motor will occur due to the difference in the rotor positions. Therefore, a damping control that can suppress these oscillations is required for the stable operation. The proposed controller consists of a speed controller for the master PMSM and a damping controller for the stable operation of two motors, designed based on sliding-mode control theory. With this nonlinear controller, robust control performance can be obtained for parameter mismatch of two motors. The feasibility of the proposed control scheme has been verified by simulation and experimental results.**

***Index Terms*—Parallel operation, permanent magnet synchronous motor (PMSM), single-inverter dual-motor drive, sliding mode control, speed control.**

I. Introduction

UTILIZATION of multimotor drive systems is required for reducing cost in applications such as conveyor belts, electric train traction, fans, etc. Multiphase inverters such as three-phase, four-phase, and five-phase inverters can be used to feed multimotor drive systems. Four- and five-phase inverters can provide independent speed control of two motors [1]–[5]. However, they require more switching devices than a three-phase inverter. Moreover, two-motor drive systems using a single three-phase inverter would offer lower economic feasibilities [6]–[8].

Single-inverter dual-induction-motor (SI-DIM) drive systems have many practical applications since the parallel operation of induction motors is naturally stable due to the presence of slip. In the SI-DIM drive system, one is assigned as the master motor of which speed is controlled, the other works as a slave in an open-loop control type [7]. Likewise, permanent magnet synchronous motors (PMSMs) can be employed for single-inverter dual-motor drive systems, denoted as SI-DPMSM. In this system, the speeds of the two motors should be equal. Besides, the direction of load torques should be the same as well. If the levels of load torques of motors are different, however, the rotor positions will be different even at the same speed. Therefore, if the same control method used in the SI-DIM is applied, the slave motor may lose synchronism, which causes instability.

To solve this problem, various control schemes have been introduced [9]–[14]. First, a selective master/slave control scheme was proposed [9], which can ensure a stable operation; if the torque angle of the motor with a higher load is controlled less than $\pi/2$, that of the motor with a lower load is naturally achieved smaller than $\pi/2$. Due to this characteristic, the motor with a higher load is assigned as the master, of which speed is controlled directly. The other motor becomes the slave and operates in an open-loop mode. This method has the advantage of being capable of controlling multiple motors in parallel. However, it requires a load torque estimation to determine which one is the master motor. Furthermore, the transient response is not good if the roles of two motors swap according to load changes.

On the other hand, there is one method where the roles of the master and slave motors are fixed regardless of the load change [10], [11]. In this method, unstable operations may occur when the load of the slave motor is higher than that of the master motor. This problem can be solved by a damping control using the P controller [10]. It is simple to implement by modifying the d-axis current reference to suppress the speed oscillation. However, if moments of inertias of the two motors are different, speed oscillations occurs.

Next, a predictive control with a cost function has been proposed [13], [14], which consists of torque errors and d-axis currents of the two motors. By minimizing the cost function, not only the stable operation but also the minimum current operation can be achieved. However, since there is no current controller, the motor current is subjected to distortions, which cause torque ripples. To solve this problem, a sophisticated algorithm is required, which makes the system control complicated [14].

The control methods introduced above cannot satisfy the control performance when the parameters of the two motors are not identical. In general, it is well known that a sliding mode control (SMC) can solve this kind of problem for power electronics applications [15]–[18].

In this article, a novel sliding-mode speed controller is proposed for the SI-DPMSM drive system, which has been expanded from the previous work [19], [20]. The proposed control

Manuscript received March 30, 2020; revised August 1, 2020; accepted September 16, 2020. Date of publication October 6, 2020; date of current version January 22, 2021. This work was supported by the Korea Institute of Energy Technology Evaluation and Planning (KETEP) and the Ministry of Trade, Industry, and Energy (MOTIE) of the Republic of Korea under Grant 20173030024770. Recommended for publication by Associate Editor U. Deshpande. *(Corresponding author: Dong-Choon Lee.)*

The authors are with the Department of Electrical Engineering, Yeungnam University, Gyeongsan 38541, South Korea (e-mail: yti1308@naver.com; dclee@yu.ac.kr).

Color versions of one or more of the figures in this article are available online at https://ieeexplore.ieee.org.

Digital Object Identifier 10.1109/TPEL.2020.3028601

scheme consists of a regular speed controller for the master motor and an additional damping controller for a stable operation of two motors. For a robust control performance against the parameter mismatch of two motors, the SMC theory, which is well known for robust control, is applied. This controller can achieve the stable operation and robust control performance in the transient as well as the steady state. In addition, a sensorless control scheme is applied for cost reduction. The feasibility of the proposed controller is verified through simulation and experimental results.

II. System Modeling

In the steady state, the voltage equations of two PMSMs are described as

$$\begin{bmatrix} V_{d1,2} \\ V_{q1,2} \end{bmatrix} = \begin{bmatrix} R_s & -\omega_{r1,2}L_s \\ \omega_{r1,2}L_s & R_s \end{bmatrix} \begin{bmatrix} i_{d1,2} \\ i_{q1,2} \end{bmatrix} + \begin{bmatrix} 0 \\ \omega_{r1,2}\phi_f \end{bmatrix} \tag{1}$$

where V_{dq} is the dq-axis stator voltage, i_{dq} is the dq-axis stator current, R_s is stator resistance, L_s is stator inductance, Φ_f is rotor flux, and ω_r is rotor speed. The subscripts 1 and 2 stand for master and slave motors, respectively. From (1), the currents of the slave motor can be expressed as

$$\begin{bmatrix} i_{d2} \\ i_{q2} \end{bmatrix} = \begin{bmatrix} R_s & -\omega_r L_s \\ \omega_r L_s & R_s \end{bmatrix}^{-1} \left(\begin{bmatrix} V_{d2} \\ V_{q2} \end{bmatrix} - \begin{bmatrix} 0 \\ \omega_{r1,2}\phi_f \end{bmatrix} \right). \tag{2}$$

Even though the speeds of the two motors are equal, the rotor phase angles may be different. Due to this difference, the voltage relationship between the two motors is expressed as

$$\begin{bmatrix} V_{d2} \\ V_{q2} \end{bmatrix} = \begin{bmatrix} \cos\Delta\theta & \sin\Delta\theta \\ -\sin\Delta\theta & \cos\Delta\theta \end{bmatrix} \begin{bmatrix} V_{d1} \\ V_{q1} \end{bmatrix} \tag{3}$$

where $\Delta\theta$ is the rotor phase angle difference between the two motors. Substituting (1) and (3) for (2)

$$\begin{bmatrix} i_{d2} \\ i_{q2} \end{bmatrix} = \begin{bmatrix} \cos\Delta\theta & \sin\Delta\theta \\ -\sin\Delta\theta & \cos\Delta\theta \end{bmatrix} \begin{bmatrix} i_{d1} \\ i_{q1} \end{bmatrix} + \frac{\omega_r\phi_f}{R_s^2 + \omega_r^2 L_s^2} \begin{bmatrix} R_s & -\omega_r L_s \\ \omega_r L_s & R_s \end{bmatrix} \begin{bmatrix} \sin\Delta\theta \\ \cos\Delta\theta - 1 \end{bmatrix}. \tag{4}$$

If the motor speed is sufficiently high, the effect of the stator resistance can be ignored. Then, (4) becomes

$$\begin{bmatrix} i_{d2} \\ i_{q2} \end{bmatrix} = \begin{bmatrix} i_{q1} & i_{d1} + \frac{\phi_f}{L_s} \\ -i_{d1} - \frac{\phi_f}{L_s} & i_{q1} \end{bmatrix} \begin{bmatrix} \sin\Delta\theta \\ \cos\Delta\theta \end{bmatrix} - \begin{bmatrix} \frac{\phi_f}{L_s} \\ 0 \end{bmatrix}. \tag{5}$$

On the other hand, the mechanical dynamic equation in (6) and motor torque equation in (7) are used to derive the state equations of the SI-DPMSM system

$$J\frac{d\omega_{r1,2}}{dt} + B\omega_{r1,2} = \frac{P}{2}T_{e1,2} \tag{6}$$

$$T_{e1,2} = \frac{3}{2}\frac{P}{2}\phi_f i_{q1,2} \tag{7}$$

where T_e is the motor torque, J is the moment of inertia, B is the friction coefficient, and P is the number of poles.

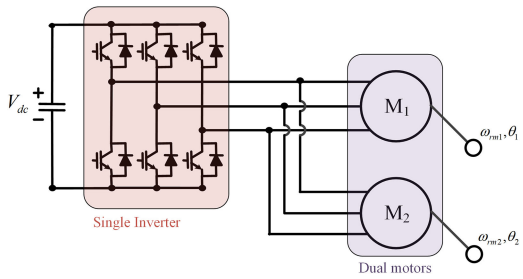

Fig. 1. Single-inverter dual-PMSM drive system with three-leg inverter.

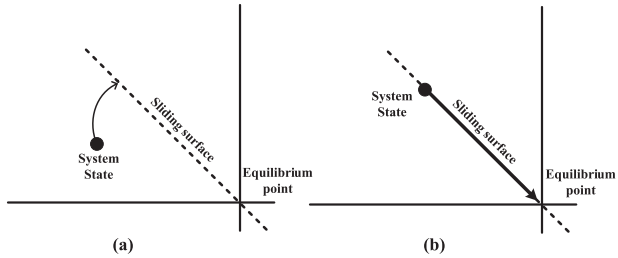

Fig. 2. Sliding mode control. (a) Reaching phase. (b) Sliding phase.

Meanwhile, the dynamic equation for the speed difference between the two motors, $\Delta\omega_r = \omega_{r2}\text{-}\omega_{r1}$, is derived from (6) as

$$\frac{d\Delta\omega_r}{dt} = -\frac{B}{J}\Delta\omega_r + \frac{1}{J}\frac{P}{2}(T_{e2} - T_{e1}). \tag{8}$$

Substituting (7) for (6) and (8), the state equation of SI-DPMSM drive system is expressed as

$$\begin{bmatrix} \dot{\omega}_{r1} \\ \Delta\dot{\omega}_r \end{bmatrix} = \begin{bmatrix} -\frac{B}{J} & 0 \\ 0 & -\frac{B}{J} \end{bmatrix} \begin{bmatrix} \omega_{r1} \\ \Delta\omega_r \end{bmatrix} + \begin{bmatrix} \frac{3P^2\phi_f}{8J} & 0 \\ -\frac{3P^2\phi_f}{8J} & \frac{3P^2\phi_f}{8J} \end{bmatrix} \begin{bmatrix} i_{q1} \\ i_{q2} \end{bmatrix} \tag{9}$$

where "$\cdot$" denotes a derivative operator.

III. Proposed Speed Controller Based on the Sliding Mode Control

A. Sliding Mode Control

The SMC is one of the nonlinear control theories, which has the advantage of being robust to parameter mismatches and disturbances. It also has the advantage of easy implementation compared with other nonlinear control theories. The SMC is composed of two modes. The first mode is the reaching phase in which the state of the system reaches the sliding surface from its initial position, as shown in Fig. 2(a). After the reaching phase mode ends, the state of the system moves to the equilibrium point, as illustrated in Fig. 2(b), named as the sliding phase. Therefore, a reaching law is needed for the state of the system to reach the sliding surface. A design procedure of a sliding mode controller using the reaching law is briefly described as follows [16].

Assume that the state equation of the system is given as

$$\dot{x} = A_0 x + B_0 u + D_0 \tag{10}$$

where x is the state variable, u is the control input, A_0 is system matrix, B_0 is input matrix, and D_0 is the disturbance. The sliding

surface can be set as

$$s = e + k_1 \int e dt \tag{11}$$

where s is the sliding surface, e ($=x-x*$) is the error of the control input, and k_1 is the integral gain. Also, the reaching law can be set as

$$\dot{s} = -k_2 \, \mathrm{sgn}(s) \tag{12}$$

where k_2 is the *sgn* function gain and the *sgn* function is defined as

$$\mathrm{sgn}(s) = \begin{cases} 1 & (s > 0) \\ 0 & (s = 0) \\ -1 & (s < 0). \end{cases} \tag{13}$$

Once the state of the system reaches the sliding surface, it has to move to the equilibrium point along the sliding surface. To examine the existence condition of the sliding mode, the Lyapunov function W is used, which is defined as

$$W = s\frac{ds}{dt}. \tag{14}$$

If the Lyapunov function in (14) is negative definite, the existence condition is satisfied. Substituting (10) for the derivative of (11) and setting it equal to (12), the SMC input is obtained as

$$u = -B_0{}^{-1}[A_0 x + D_0 - \dot{x}^* + k_1 e + k_2 \mathrm{sgn}(s)]. \tag{15}$$

B. Design of Speed Controller

To design the speed controller based on the SMC, the sliding surface has to be determined at first. In this article, a single integral sliding surface is selected by

$$\begin{bmatrix} s_s \\ s_d \end{bmatrix} = \begin{bmatrix} e_1 + k_{s1} \int e_1 dt \\ e_2 + k_{d1} \int e_2 dt \end{bmatrix} \tag{16}$$

where s_s and s_d represent the sliding surfaces of the master speed controller and the damping controller, respectively, $e_1 = \omega_{r1} - \omega_{r1}*$ is the speed error of the master motor, and $e_2 = \Delta\omega_r - \Delta\omega_r*$ is the speed difference error between the two motors; and k_{s1} and k_{d1} are the integral gains for speed control and damping control, respectively. However, since the speeds of two motors are equal, the reference of the speed difference between the two motors is set as zero ($e_2 = \Delta\omega_r$).

On the other hand, a reaching law should be determined so that the state of the system can reach a sliding surface given in (16), which is set as

$$\begin{bmatrix} \dot{s}_s \\ \dot{s}_d \end{bmatrix} = \begin{bmatrix} -k_{s2}\mathrm{sgn}(s_s) - \rho s_s \\ -k_{d2}\mathrm{sgn}(s_d) \end{bmatrix} \tag{17}$$

where k_{s2} and k_{d2} are the *sgn* function gains for speed control and damping control, respectively.

In (17), the reaching law of the speed controller of the master motor consists of the *sgn* function and an additional term of -ρs_s, [22]. If the reaching law is set only with the *sgn* function without the sliding surface, the value of k_{s2} determines the speed at which the state of the system reaches the sliding surface and the magnitude of chattering. If k_{s2} is high, the time to reach the sliding surface is short; however, a severe chattering phenomenon exists at steady state. If k_{s2} is low, the chattering decreases but the speed response becomes sluggish. In the proposed system, for example, when the damping gain k_{d2} is high, the speed difference between the two motors converges to zero quickly; however, a chattering in i_{d1} occurs. Conversely, when k_{d2} is low, the chattering does not occur, but the speed difference converges to zero slowly. For this reason, the additional term, $-\rho s_s$, in (17) is crucial to improve the speed response. To reduce the chattering further, the *sgn* function is replaced by the hyperbolic tangent [17]. Then, the reaching law is modified as

$$\begin{bmatrix} \dot{s}_s \\ \dot{s}_d \end{bmatrix} = \begin{bmatrix} -k_{s2}\tanh(s_s) - \rho s_s \\ -k_{d2}\tanh(s_d) \end{bmatrix}. \tag{18}$$

Next, from (15), (16), and (18), the existence condition of the sliding modes for the proposed speed controller is expressed as

$$\begin{aligned} W &= \begin{bmatrix} s_s \\ s_d \end{bmatrix}^T \begin{bmatrix} -k_{s2}\mathrm{sgn}(s_s) - \rho s_s \\ -k_{d2}\mathrm{sgn}(s_d) \end{bmatrix} \\ &= -k_{s2}s_s\mathrm{sgn}(s_s) - \rho s_s^2 - k_{d2}s_d\mathrm{sgn}(s_d). \end{aligned} \tag{19}$$

Since $s_s sgn(s_s) > 0$ and $s_d sgn(s_d) > 0$, the Lyapunov function is negative definite when k_{s2}, k_{d2}, and ρ are positive. In this case, the proposed sliding mode speed controller is asymptotically stable. To derive the control input of the sliding mode speed controller, substituting (9) for the derivative of (16)

$$\begin{aligned} \begin{bmatrix} \dot{s}_s \\ \dot{s}_d \end{bmatrix} &= \begin{bmatrix} -\frac{B}{J} & 0 \\ 0 & -\frac{B}{J} \end{bmatrix} \begin{bmatrix} \omega_{r1} \\ \Delta\omega_r \end{bmatrix} + \begin{bmatrix} \frac{3P^2\phi_f}{8J} & 0 \\ -\frac{3P^2\phi_f}{8J} & \frac{3P^2\phi_f}{8J} \end{bmatrix} \begin{bmatrix} i_{q1} \\ i_{q2} \end{bmatrix} \\ &\quad + \begin{bmatrix} -\dot{\omega}_{r1}^* + k_{s1}e_1 \\ k_{d1}e_2 \end{bmatrix}. \end{aligned} \tag{20}$$

By comparing (20) with (18), the resultant control input of the sliding mode speed controller is obtained as

$$\begin{aligned} \begin{bmatrix} i_{q1}^* \\ i_{q2}^* \end{bmatrix} &= \frac{8}{3P^2\phi_f} \\ &\quad \times \left(\begin{bmatrix} B & 0 \\ B & B \end{bmatrix} \begin{bmatrix} \omega_{r1} \\ \Delta\omega_r \end{bmatrix} - \begin{bmatrix} J(-\dot{\omega}_{r1}^* + k_{s1}e_1) \\ J(-\dot{\omega}_{r1}^* + k_{s1}e_s + k_{d1}e_2) \end{bmatrix} \right) \\ &\quad + \begin{bmatrix} -k_{s2}\tanh(s_s) - \rho s_s \\ -k_{s2}\tanh(s_s) - \rho s_s - k_{d2}\tanh(s_d) \end{bmatrix}. \end{aligned} \tag{21}$$

The output of the sliding mode speed controller is the q-axis current references of the master and slave motors. In this article, since the fixed master/slave control scheme is used, the master motor currents are controlled directly, but not for the slave motor currents. By (5), the q-axis current reference of the slave motor, i_{q2}^* is referred to the d-axis current reference of the master motor i_{d1}^*, which is controlled directly. Resultantly, the d-axis current reference of the master motor is obtained as

$$i_{d1}^* = \frac{-i_{q2}^* + i_{q1}\cos\Delta\theta - \frac{\phi_f}{L_s}\sin\Delta\theta}{\sin\Delta\theta}. \tag{22}$$

Fig. 3 shows the block diagram of the proposed sliding mode speed controller, where the upper and lower parts represent the speed controller of the master motor and the damping controller for stable parallel operation, respectively.

III. Sensorless Control

For a low-cost implementation, the SI-DPMSM drive system needs a sensorless control. In this article, a simple sensorless algorithm based on the Luenberger observer is applied [10], [21], which has the advantage in computation time.

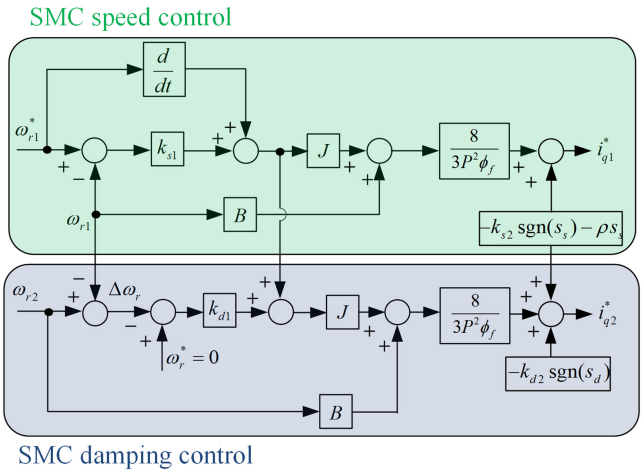

Fig. 3. Proposed sliding mode speed controller.

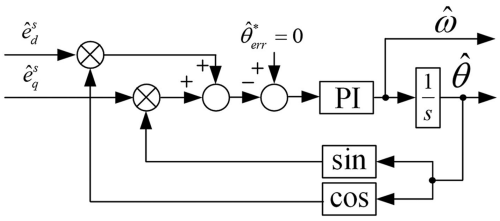

Fig. 4. Block diagram of speed and rotor position estimation [10].

The Luanberger observer is expressed in a discrete time domain as

$$\begin{bmatrix} z_n(k+1) \\ z_u(k+1) \end{bmatrix} = \begin{bmatrix} dT_s+1 & 0 \\ 0 & dT_s+1 \end{bmatrix} \begin{bmatrix} z_n \\ z_u \end{bmatrix} + T_s \begin{bmatrix} d & -\omega_r \\ \omega_r & d \end{bmatrix} \begin{bmatrix} (R_s+dL_s)i_q^s - v_q^s \\ (R_s+dL_s)i_d^s - v_d^s \end{bmatrix}. \tag{23}$$

where T_s is the sampling time, d is the observer gain, and z is an auxiliary variable defined as

$$\begin{bmatrix} z_n \\ z_u \end{bmatrix} = \begin{bmatrix} e_q^s \\ e_d^s \end{bmatrix} - L_s \begin{bmatrix} d & -\omega_r \\ \omega_r & d \end{bmatrix} \begin{bmatrix} i_q^s \\ i_d^s \end{bmatrix} \tag{24}$$

where e_q^s and e_d^s are dq-axes back-EMFs, and i_q^s and i_d^s are dq-axes currents in the stationary reference frame. Substituting (23) for (24), the back-EMFs can be estimated as

$$\begin{bmatrix} \hat{e}_q^s(k+1) \\ \hat{e}_d^s(k+1) \end{bmatrix} = \begin{bmatrix} z_n(k+1) \\ z_u(k+1) \end{bmatrix} + L_s \begin{bmatrix} d & -\omega_r \\ \omega_r & d \end{bmatrix} \begin{bmatrix} i_q^s \\ i_d^s \end{bmatrix}. \tag{25}$$

From the estimated back-EMFs, the rotor speed and position of the motors are obtained through the phase-lock-loop (PLL), as shown in Fig. 4, where the estimated position error is expressed as

$$\hat{\theta}_{err} = \hat{e}_q^s \cos\hat{\theta} + \hat{e}_d^s \sin\hat{\theta} = \hat{\omega}\sin(\hat{\theta}-\theta). \tag{26}$$

By controlling $\hat{\theta}_{err}$ to be zero, the rotor position can be obtained.

Fig. 5 shows the overall control block diagram of the SI-DPMSM drive system. The outputs of the proposed speed controller are the q-axis current references of two PMSMs.

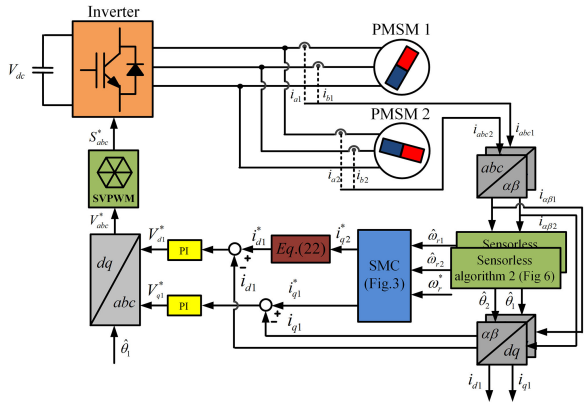

Fig. 5. Control block diagram of the proposed SI-DPMSM drive.

TABLE I
PARAMETERS OF PMSM

Parameter	VALUE	Symbol
Rated power [W]	450	P_{rated}
Rated voltage [V]	102.8	v_s
Rated current [A]	3.23	i_s
Rated torque [N·m]	2.15	T_e
Rated speed [rpm]	2000	ω_{rm}
Back-EMF constant [V_{pk}/krpm]	61.13	k_e
Number of poles	8	P
Moment of inertia [kg·m^2 x 10^{-4}]	1.092	J
Friction coefficient [N·m·s]	3.276e-5	B
Stator resistance [Ω]	0.993	R_s
Stator inductance [mH]	6.71	L_s

For speed and rotor position estimation, the currents of both motors are needed.

IV. SIMULATION RESULTS

Using the PSIM software, simulations have been carried out to verify the validity of the proposed controller. Table I lists the parameters of the PMSMs used in the simulation. The switching frequency of the inverter is 5 kHz and the controller gains are set as follows: $k_{s1}=10$, $k_{s2}=0.1$, $k_{d1}=0.1$, $k_{d2}=10$ and $\rho=0.11$. The bandwidth of the current control loop is set as 700 Hz, which yields the PI controller gains as $k_{cp}=30$ and $k_{ci}=4468$. All the SMC gains are determined by a trial and error, which satisfy the Lyapunov's existence condition.

Fig. 6 shows the speed responses for step changes of its reference from 1000 to 1500 r/min and back to 1500 r/min, where the load torques of the master and slave motors are 1 and 1.5 N·m, respectively. The speed control performance is satisfactory with a little overshoot and undershoot. The sliding surface of the speed controller s_s, has some transients due to the change of the speed reference. However, that of the damping controller s_d, is kept constant since the load is not changed during transient conditions.

Fig. 7 shows the speed responses when the load of the master motor is kept constant at 1 N·m and that of the slave motor changes from no load to 1.5 N·m and back to no load. Fig. 7(a) shows the speeds of two motors. Due to the damping control,

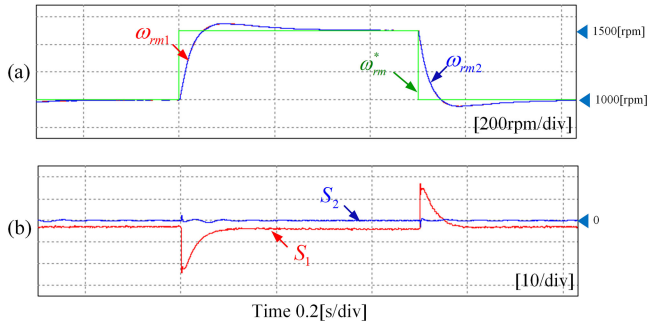

Fig. 6. Speed responses with step changes in its reference. (a) Two motor speeds and reference. (b) Sliding surfaces.

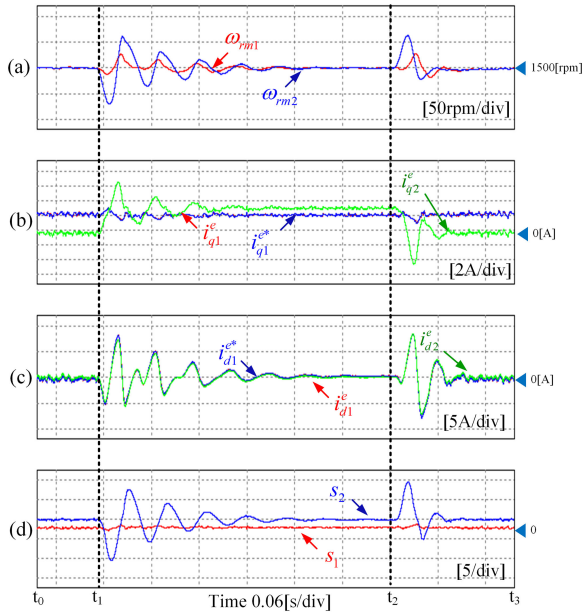

Fig. 7. Speed responses (T_{L1}: 1 N·m, T_{L2}: no load → 1.5 N·m → no load). (a) Two motor speeds. (b) q-axis currents. (c) d-axis currents. (d) Sliding surfaces.

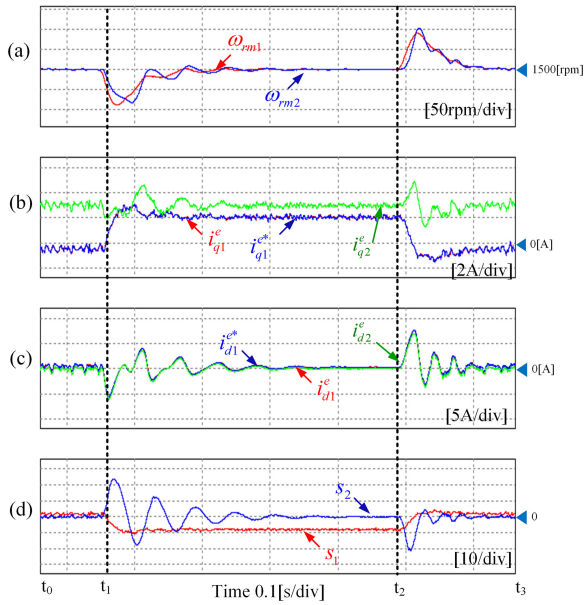

Fig. 8. Speed responses (T_{L1} : no load → 1 N·m → no load, T_{L2} : 1.5 N·m). (a) Two motor speeds. (b) q-axis currents. (c) d-axis currents. (d) Sliding surfaces.

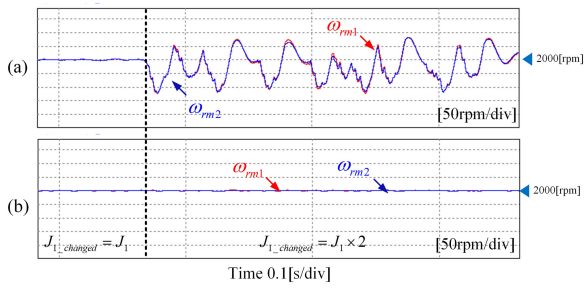

Fig. 9. Speed control performance for a change of J in the controller ($J_{1\cdot\text{changed}} = J_1 \times 2$). (a) Conventional method. (b) Proposed method.

both motors operate stably even though the load of the slave motor changes. Fig. 7(b) and (c) shows the dq-axes currents of two motors. From t_0 to t_1, a load is applied to the master motor only, where the q-axis current of the master motor i_{q1} is 2 A and that of the slave motor i_{q2} is 0 A and the rotor angle difference between two motors $\Delta\theta$ is 0.1714 rad. From (22), the d-axis current of the master motor i_{d1} is calculated as -0.86 A. From t_1 to t_2, both motors are loaded, where $i_{q1} = 2.2$ A, $i_{q2} = 3.1$ A, and $\Delta\theta = -0.0626$ rad. From (22), $i_{d1} = 0.01$ A. Finally, from t_2 to t_3, the load condition is the same as that of in the first interval from t_0 to t_1. Fig. 7(d) shows the sliding surfaces of the speed controller and the damping controller. The sliding surface of the master motor has no transient state since there is no load variation; however, the transient state appears in that of the damping controller since the load of the slave motor has changed.

Fig. 8 shows the speed responses when the load of the slave motor is kept constant at 1 N·m and that of the master motor changes from no load to 1.5 N·m and back to no load. Fig. 8(a) shows the responses of the motor speeds. Fig. 8(b) and (c) shows the dq-axes currents of two motors. From t_0 to t_1, a load is applied to the slave motor only. So, the q-axis current of the master motor $i_{q1} = 0$ A the q-axis current of slave motor $i_{q2} = 3$ A, and the rotor angle difference between two motors $\Delta\theta = -0.227$ rad. Therefore, the d-axis current of the master motor $i_{d1} = 0.66$ A is obtained from (22).

From t_1 to t_2, both motors are loaded, where $i_{q1} = 2$ A, $i_{q2} = 3$ A, and $\Delta\theta = -0.0638$ rad. By (22), $i_{d1} = 0.012$ A. Finally, from t_2 to t_3, the load condition is the same as that of in the first interval from t_0 to t_1, where $i_{d1} = 0.66$ A. Fig. 8(d) shows the sliding surfaces of the two controllers. Since the load variations in the master motor exist, transient states occur in the sliding surface of the speed controller. Moreover, the transient responses also appear in the sliding surface of the damping controller to make the slave motor speed equal to the same as that of the master motor.

Fig. 9 shows the speed control performance when the moment of inertia (J_1) in the master motor speed controller is set as double. Since the real moment of inertia is fixed in the experiment, the value of J_1 needed to determine the speed controller gain is changed. In the conventional method, the speed oscillation occurs when the parameter is changed. However, with the proposed method, the speed oscillation does not occur.

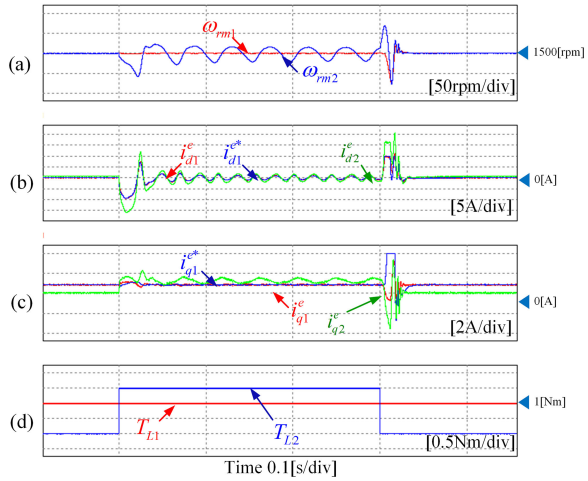

Fig. 10. Performances for parameter mismatch with conventional method ($L_{s1\_changed} = L_{s1} \times 1.5$). (a) Two motor speeds. (b) d-axis currents. (c) q-axis currents. (d) Load torques.

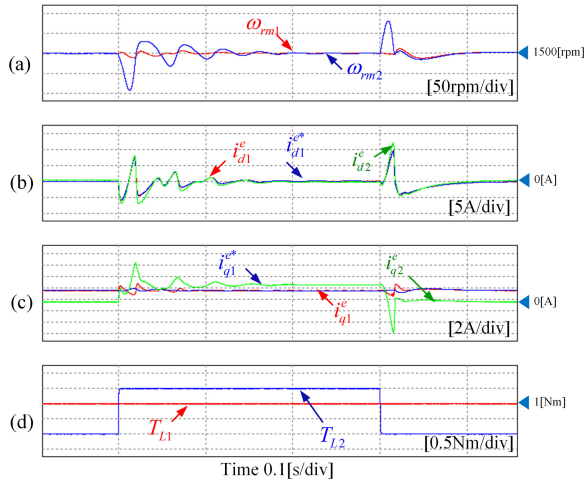

Fig. 11. Performances for parameter mismatch with proposed method ($L_{s1\_changed} = L_{s1} \times 1.5$). (a) Two motor speeds. (b) d-axis currents. (c) q-axis currents. (d) Load torques.

Then, the control performance in the case of a 50% mismatch in L_s is shown in Figs. 10 and 11, where the measured speed is used for control to exclude the effect of the speed estimation performance. In Fig. 10(a), the oscillation in the slave motor speed occurs with the conventional method. However, the proposed method gives better speed control performance, as shown Fig. 11(a).

VI. Experimental Results

To verify the feasibility of the proposed control method, the hardware test has been carried out. The motor parameters are the same as those of in the simulation (listed in Table I). An inverter was assembled from the PM75RL1A060 (Mitsubishi) IPM modules together with the TMS320F28335 control board (Texas-Instrument). Besides, the four current sensors, two for each motor, were used to measure motor currents and one voltage sensor for measuring the dc-link voltage. The load application was made by connecting a resistor through the diode rectifier

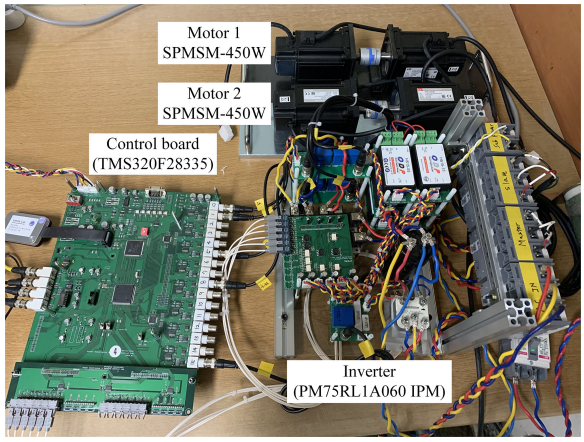

Fig. 12. Experimental setup.

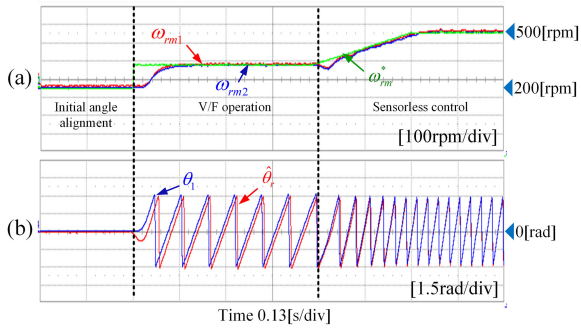

Fig. 13. Start-up operation. (a) Motor speeds. (b) Rotor positions.

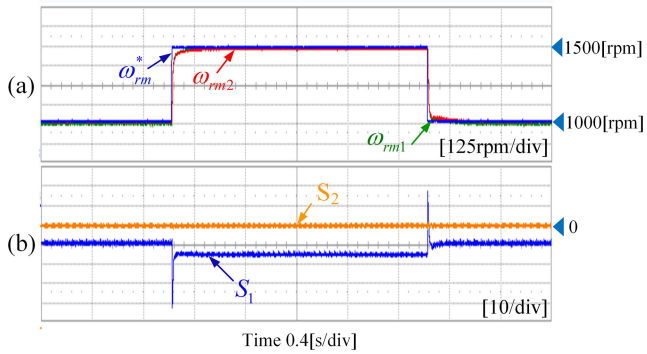

Fig. 14. Speed responses with step changes in reference. (a) Two motor speeds and references. (b) Sliding surfaces.

to the generator, which is mechanically coupled with the motor shaft. The controller gains are also the same as those in the simulation. Fig. 12 shows the hardware setup.

Fig. 13 shows the initial start-up process of the PMSM drive system for a test. The performance of the simple sensorless scheme based on the back-EMF estimation is not good at low speeds [21]. For starting, hence, the V/F control is applied from the standstill condition up to 200 r/min, which is 10% of the rated speed.

Then, the sensorless vector control is applied with the estimated speed and rotor position.

Fig. 14 shows the speed responses with regard to its reference changes. Similarly to the simulation results, the sliding surface

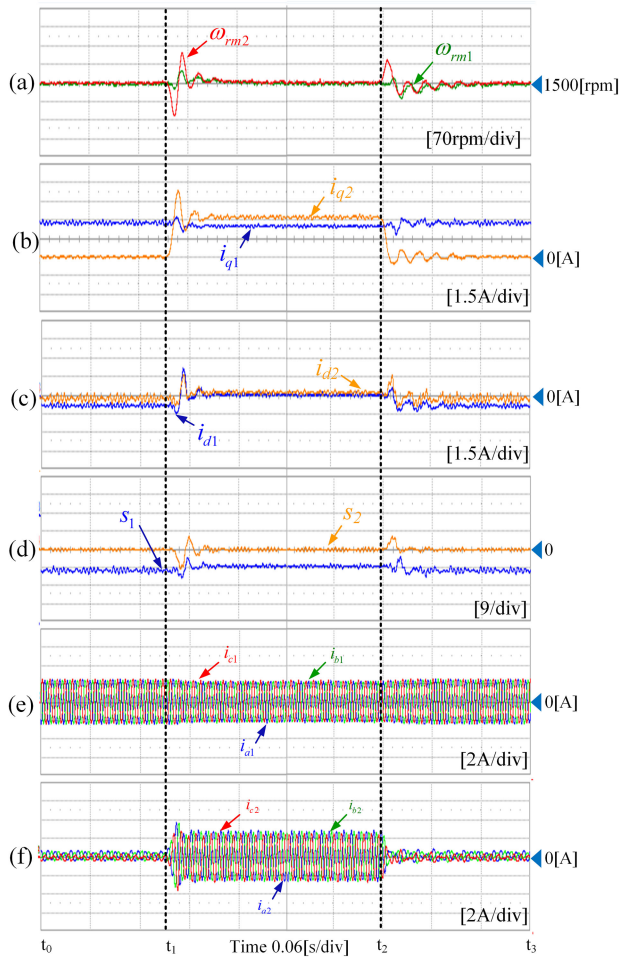

Fig. 15. Speed responses (T_{L1} : 1 N·m, T_{L2} : no load → 1.5 N·m → no load). (a) Two motor speeds. (b) q-axis currents. (c) d-axis currents. (d) Sliding surfaces. (e) Master motor currents. (f) Slave motor currents.

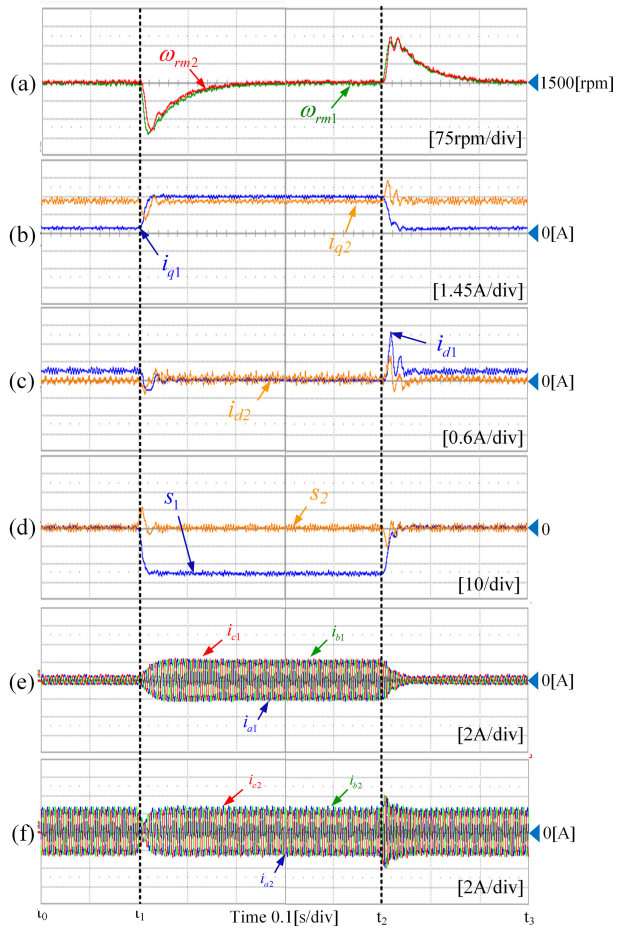

Fig. 16. Speed responses (T_{L1} : no load → 1 N·m → no load, T_{L2} : 1.5 N·m). (a) Two motor speeds. (b) q-axis currents. (c) d-axis currents. (d) Sliding surfaces. (e) Phase currents of master motor. (f) Phase currents of slave motor

of the damping controller s_d, is zero; however, the transient responses appear in the sliding surface of the speed controller s_s, according to the speed change.

Fig. 15 shows the experimental results corresponding to Fig. 7. Before applying a load to the slave motor (t_0~t_1), the load difference between the two motors is large. Therefore, the d-axis current of the master motor is controlled at the value determined in (22), as shown in Fig. 15(c). Fig. 15(d) shows the sliding surfaces of the two controllers. They seem to be similar to the simulation results, but some transient responses appear in the sliding surface of the speed controller s_s. While both motors are loaded (t_1~t_2), the d-axis current of the master motor is near zero since the load difference between them is small. In addition, Fig. 15(e) and (f) shows the phase currents of the master and slave motors, respectively.

Fig. 16 shows the speed responses corresponding to Fig. 8. Similarly to the previous results, from t_0 to t_1, a load is applied to the slave motor only. Therefore, the d-axis current of the master motor i_{d1} is controlled at the value determined in (22), which is shown in Fig. 16(c). In this duration, i_{d1} is controlled to make the speed difference of two motors be a zero. When the load of the master motor is changed, a transient state appears in the sliding surfaces of the speed controller, as shown in Fig. 16(d).

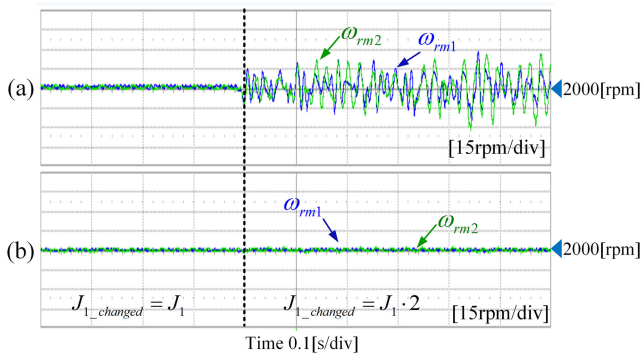

Fig. 17. Speed control performance for parameter mismatch ($J_{1\_changed} = J_1 \times 2$). (a) Conventional method. (b) Proposed method.

In addition, the phase currents of the master and slave motors are shown in Fig. 16(e) and (f), respectively.

Fig. 17 shows the speed control performance of two motors as the moment of inertia of the master motor is doubled. To realize the parameter mismatch in the test, J_1 used to determine the speed controller gain of the master motor is changed two times, both the conventional and proposed control methods work well. When J_1 is increased, speed oscillations occur for the

conventional scheme, as shown in Fig. 17(a). On the contrary, the proposed scheme works well without any oscillation, as shown in Fig. 17(b).

VII. Conclusion

This article has proposed a novel sliding mode speed controller for parallel operation of dual-PMSM drives fed by a single inverter. The proposed controller consists of a speed controller for the master motor speed control and a damping controller, which can ensure the stable parallel operation. Simulation and experimental results for a 450-W dual-PMSM drive system have verified the effectiveness of the proposed controller under speed reference changes and load variations. Furthermore, even with different moments of inertias, the proposed control scheme works well without any speed oscillation.

References

[1] S. Ito, T. Moroi, Y. Kubo, K. Matsuse, and K. Rajashekara, "Independent control of two permanent-magnet synchronous motors fed by a for-leg inverter," *IEEE Trans. Ind. Appl.*, vol. 51, no. 1, pp. 753–760, Jan./Feb. 2015.

[2] G. J. Su and J. S. Hsu, "A five-leg inverter for driving a traction motor and a compressor motor," *IEEE Trans. Power Electron.*, vol. 21, no. 3, pp. 687–692, May 2006.

[3] L. Tang and G. J. Su, "High-performance control of two three-phase permanent-magnet synchronous machines in an integrated drive for automotive applications," *IEEE Trans. Power Electron.*, vol. 23, no. 6, pp. 3047–3055, Nov. 2008.

[4] J. Sabarad, G. H. Kulkami, and S. Sattigeri, "Dual three phase induction motor control using five leg inverter," in *Proc. IEEE Int. Conf. Smart grids, Power Adv. Control Engineer*, 2017, pp. 120–125.

[5] Y. Mei, Z. Yi, and Z. Li, "A two-step model predictive control strategy for dual induction motor drive system fed by five-leg inverter," in *Proc. IEEE 18th Int. Conf. Elect. Mach. Syst.*, 2015, pp. 137–142.

[6] B. M. Joshi, D. C. Patel, and M. C. Chandorkar, "Machine interaction in field oriented controlled multi-machine three phase induction motor drives," in *Proc. IEEE Int. Elect. Mach. Drives Conf.*, 2011, pp. 342–347.

[7] K. Matsuse, H. Kawai, Y. Kouno, and J. Oikawa, "Characteristics of speed sensorless vector controlled dual induction motor drive connected in parallel fed by a single inverter," *IEEE Trans. Ind. Appl.*, vol. 40, no. 1, pp. 153–161, Jan./Feb. 2004.

[8] F. Xu, L. Shi, and Y. Li, "The weighted vector control of speed irrelevant dual induction motors fed by single inverter," *IEEE Trans. Power Electron.*, vol. 28, no. 12, pp. 5665–5672, Dec. 2013.

[9] D. Bidart, M. P. David, P. Maussion, and M. Fadel, "Mono inverter multi-parallel magnet synchronous motor: Structure and control strategy," *IET Elect. Power Appl*, vol. 5, no. 3, pp. 1103–1108, Mar. 2001.

[10] Y. Lee and J.. Ha, "Control method for mono inverter dual parallel surface mounted permanent magnet synchronous machine drive system," *IEEE Trans. Ind. Electron.*, vol. 64, no. 10, pp. 6096–6107, Oct. 2015.

[11] Y. Lee and J. Ha, "Control method of mono inverter dual parallel drive system with interior permanent magnet synchronous machines," *IEEE Trans. Power Electron*, vol. 31, no. 10, pp. 7077–7086, Oct. 2016.

[12] C. Yun and W.-H. Kwon, "The resonance characteristic analysis for speed control of parallel connected dual SPMSMs fed by a single inverter," *Trans. Korean Inst. Elect. Eng.*, vol. 66, no. 4, pp. 643–650, Apr. 2017.

[13] N. L. Nguyen, M. Fadel, and A. Llor, "A new approach to predictive torque control with dual parallel PMSM system," in *Proc. IEEE Int. Conf. Ind. Technol.*, 2013, pp. 1806–1811.

[14] M. Fadel, N. L. Nguyen, and A. Llor, "Different solutions of predictive control for two synchronous machines in parallel," in *Proc. IEEE Int. Symp. Sensorless Control Elect. Drives Predictive Control Elect. Drives Power Electron.*, 2013, pp. 1–7.

[15] Y. Jeung and D. Lee, "Voltage and current regulations of bidirectional isolated dual-active-bridge DC-DC converters based on a double-integral sliding mode control," *IEEE Trans. Power Electron*, vol. 34, no 7, pp. 6937–6946, Jul. 2019.

[16] X. Zhang, L. Sun, K. Zhao, and L. Sun, "Nonlinear speed control for PMSM system using sliding mode control and disturbance compensation techniques," *IEEE Trans. Power Electron*, vol. 28, no. 3, pp. 1358–1365, Sep. 2013.

[17] J. Hu, H. Zian, B. Hu, Y. He, and Z. Q. Zhu, "Direct active and reactive power regulation of DFIG using sliding mode control approach," *IEEE Trans. Energy Convers.*, vol. 25, no. 4, pp. 1028–1039, Dec. 2010.

[18] B. Wang, C. Wnag, Q. Hu, G. Ma, and J. Zhou, "Adaptive sliding mode control with enhanced optimal reaching law for boost converter based hybrid power sources in electric vehicles," *J. Power Electron.*, vol. 9, no. 2, pp. 549–559, Mar. 2019.

[19] T.-I. Yeam and D.-C. Lee, "Speed control of single inverter dual PMSM drives using sliding mode control," in *Proc. IEEE Vehicle Power Propulsion Conf.*, 2019, pp. 1–6.

[20] T.-I. Yeam, "Sliding mode speed controller for parallel operation of two permanent magnet synchronous motors with single inverter," M.S. thesis, Yeungnam Univ., Gyeongsan, South Korea, 2020.

[21] J. S. Kim and S. K. Sul, "High performance PMSM drives without rotational position sensors using reduced order observer," in *Proc. IEEE-IAS Annu. Meeting*, 1995, pp. 75–82.

[22] J. Y. Hung, Q. Gao, and J. C. Hung, "Variable structure control: A survey," *IEEE Trans. Ind. Electron*, vol. 40, no. 1, pp. 2–22, Feb. 1993.

[23] X. Wing, Z. Wang, Z. Xu, J. He, and W. Zhao, "Diagnosis and tolerance of common electrical faults in T-type three-level inverters fed dual three-phase PMSM drives," *IEEE Trans. Power Electron*, vol. 35, no. 2, pp. 1753–1769, Feb. 2020.

[24] L. Gou, C. Wang, M. Zhou, and X. You, "Integral sliding mode control for starting speed sensorless controlled induction motor in the rotating condition," *IEEE Trans. Power Electron*, vol. 35, no. 4, pp. 4105–4116, Apr. 2020.

[25] Y. Wang, Y. Xu, and J. Zou, "Sliding-mode sensorless control of PMSM with inverter nonlinearity compensation," *IEEE Trans. Power Electron*, vol. 34, no. 10, pp. 10206–10220, Oct. 2019.

[26] S. Kwon and J.-I. Ha, "Fault-Tolerant operation under single-phase open in mono inverter dual parallel SMPSMSM with single shaft," *IEEE Trans. Power Electron*, vol. 34, no. 12, pp. 12064–12079, Dec. 2019.

[27] L. Feng, M. Deng, S. Xu, and D. Huang, "Speed regulation for PMSM drives based on a novel sliding mode controller," *IEEE Access*, vol. 8, pp. 63577–63584, Mar. 2020.

Tae-Il Yeam (Student Member, IEEE) received the B.S. and M.S. degrees in electrical engineering from Yeungnam University, Gyeongsan, South Korea, in 2018 and 2020, respectively.

His current research interests include power electronics and motor drive systems.

Dong-Choon Lee (Senior Member, IEEE) received the B.S., M.S., and Ph.D. degrees in electrical engineering from Seoul National University, Seoul, South Korea, in 1985, 1987, and 1993, respectively.

He was a Research Engineer with Daewoo Heavy Industry, South Korea, from 1987 to 1988. He has been a Faculty Member with the Department of Electrical Engineering, Yeungnam University, Gyeongsan, South Korea, since 1994. He was a Visiting Scholar with the Power Quality Laboratory, Texas A&M University, College Station, TX, USA, in 1998; the Electrical Drive Center, University of Nottingham, Nottingham, ENG, UK, in 2001; the Wisconsin Electric Machines and Power Electronics Consortium, University of Wisconsin, Madison, WI, USA, in 2004; and the FREEDM Systems Center, North Carolina State University, Raleigh, NC, USA, from September 2011 to August 2012. He served as the Editor-in-Chief of the *Journal of Power Electronics* of the Korean Institute of Power Electronics (KIPE), from January 2015 to December 2017. In 2019, he was the President of KIPE. His current research interests include power converter design and control, renewable energy and its grid connection, ac machine drives, and dc power systems.